

Many particle entanglement in two-component Bose-Einstein Condensates

A. Micheli¹, D. Jaksch¹, J. I. Cirac^{1,2}, and P. Zoller¹

¹*Institut für Theoretische Physik, Universität Innsbruck, A-6020 Innsbruck, Austria*

²*Max-Planck Institut für Quantenoptik, Hans-Kopfermann Str. 1, D-85748 Garching, Germany*

(Dated: June 5, 2018)

We investigate schemes to dynamically create many particle entangled states of a two component Bose-Einstein condensate in a very short time proportional to $1/N$ where N is the number of condensate particles. For small N we compare exact numerical calculations with analytical semiclassical estimates and find very good agreement for $N \geq 50$. We also estimate the effect of decoherence on our scheme, study possible scenarios for measuring the entangled states, and investigate experimental imperfections.

PACS numbers: 03.75.Fi, 42.50.-p, 42.50.Ct

I. INTRODUCTION

The creation of many particle entangled states in macroscopic systems is one of the major goals in the studies on fundamental aspects of quantum theory [1, 2, 3, 4, 5]. The notion of entanglement in macroscopic ensembles allows to investigate the boundary between quantum physics and classical physics and, possibly, could also give some insight into the measurement process [6, 7, 8]. The experimental creation of many particle entanglement could also lead to the realization of several of the “Gedankenexperiments” proposed in the early days of quantum theory [9]. Also, apart from the fundamental physical interest in entanglement, the whole field of quantum computing and quantum information is based upon the ability to create and control entangled states [10].

The experimental achievement of atomic Bose-Einstein condensation (BEC) [11] has opened fascinating possibilities for studying quantum properties of a macroscopic number of cold quantum degenerate atoms in the laboratory. Interesting aspects of many particle entanglement can be studied by using condensates with internal degrees of freedom [12, 13, 14, 15, 16, 17, 18]. For instance, it has been shown that the coherent collisional interactions in a BEC allow to generate substantial many-particle entanglement in the spin degrees of freedom of a two-component condensate [12] during the free evolution of the condensates.

The extremely long coherence time in a BEC is one of the key features making the proposals for engineering many particle entanglement in a BEC feasible [19]. However, one still has to make sure that (i) the creation of the many particle entangled state takes place on a time scale much shorter than the coherence time, and (ii) the produced many particle entangled states are robust against decoherence, i.e., particle loss should not destroy the entanglement.

In this paper we will investigate in detail a scheme that allows to create many particle entangled states in a two-component BEC interacting with a classical laser field or microwave field on a time scale proportional to $1/N$ with N the number of condensate particles (see also [20]). Let us briefly explain the basic idea of this scheme. If we

concentrate on the dynamics of the internal states of the condensate (e.g. atomic hyperfine levels) the Hamiltonian H of the system is given by (cf. Sec. II A 3)

$$H = \chi S_z^2 + \Omega S_x, \quad (1)$$

where χ is determined by the interaction strengths between the condensate particles and Ω is the Rabi frequency of the external field interacting with the condensate. Here the angular momentum operator $\mathbf{S} = \{S_x, S_y, S_z\}$ is defined by

$$\begin{aligned} S_x &= \frac{1}{2}(a^\dagger b + b^\dagger a), \\ S_y &= \frac{i}{2}(b^\dagger a - a^\dagger b), \\ S_z &= \frac{1}{2}(a^\dagger a - b^\dagger b), \end{aligned}$$

where a (b) are bosonic destruction operators for particles in internal state A (B) with a fixed spatial mode function $\psi_{A(B)}$. We consider the situation, where initially all the condensate particles are in internal state $|A\rangle$. This state corresponds to an eigenstate of S_z with eigenvalue $N/2$. Then a $\pi/2$ pulse is applied to the condensate which brings each particle in a superposition state $(|A\rangle + |B\rangle)/\sqrt{2}$ corresponding to an eigenstate of S_x with eigenvalue $N/2$. The internal wave function $|\Psi\rangle$ of the condensate is thus given by

$$|\Psi(t=0)\rangle = \frac{1}{\sqrt{2^N N!}} (a^\dagger + b^\dagger)^N |vac\rangle, \quad (2)$$

where $|vac\rangle$ is the vacuum state.

To get a qualitative understanding of the subsequent time evolution of $|\Psi(t)\rangle$ we use the familiar phase model [21, 22] where one replaces $S_z \rightarrow -i\partial_\phi$ and $S_x \rightarrow N/2 \cos \hat{\phi}$, with ϕ the relative phase between the two condensate components, in the Hamiltonian and finds (cf. Sec. II B)

$$H_\phi = -\chi \frac{\partial^2}{\partial \phi^2} + \frac{\Omega N}{2} \cos \hat{\phi}. \quad (3)$$

We note that the eigenstates of $\hat{\phi}$ given by $|\phi\rangle \sim \sum_m e^{-im\phi} |N/2 - m\rangle_A |N/2 + m\rangle_B$ are entangled states

of particles in states A and B [22, 23, 24]. Projection on these eigenstates gives the phase wave function $\Psi(t, \phi) = \langle \phi | \Psi(t) \rangle$. For large condensate particle number N the phase wave function corresponding to the initial state $\Psi(0, \phi)$ is well approximated by a narrow Gaussian wave-packet with a width of $\sigma = 1/\sqrt{N}$ centered at $\phi = 0$, i.e. a maximum of the phase potential $V(\hat{\phi}) = \Omega S \cos \hat{\phi}$ as schematically shown in Fig. 1a. The time evolution due to H_ϕ will first squeeze this wave packet due to the harmonic terms of $V(\hat{\phi})$ resulting in an increased width. Then the anharmonicity of $V(\hat{\phi})$ becomes important and the wave packet splits up as shown in Fig. 1b. These two wave packets correspond to wave packets of opposite relative particle number (measured by S_z) since they move in opposite direction. Their superposition is thus a macroscopically entangled state. In the remainder of this paper we will investigate the process described above quantitatively. In particular, we will use a semiclassical approximation which allows to analytically estimate properties of the many particle entangled states like the positions of maxima in the relative particle number distribution.

The paper is organized as follows: In Sec. II we will introduce the model. We derive a two mode Hamiltonian describing a two component condensate interacting with a laser or microwave field. Then we discuss the phase model already used in the introduction and present a semiclassical model. In Sec. III we define the most common types of many particle entangled states and give a short overview of recent proposals for entanglement creation in BEC's. We present our results in Sec. IV and Sec. V where we compare the properties of the many particle entangled states found by numerical solution of the exact Schrödinger equation with the semiclassical estimates. Furthermore in Sec. VI we improve the scheme by one-axis-pre-squeezing. Finally, in Sec. VII we discuss the stability of the many particle entangled states under decoherence and investigate possible measurement strategies to identify the entangled states. Also we study the influence of imperfections in the external field on our scheme.

II. MODEL

In this section we present the model used to study the two component condensate interacting with an external field. We write down the Hamiltonian for this system and use the two mode approximation to obtain a simplified description of the system in terms of angular momentum operators. Then we introduce the phase model and a semiclassical model.

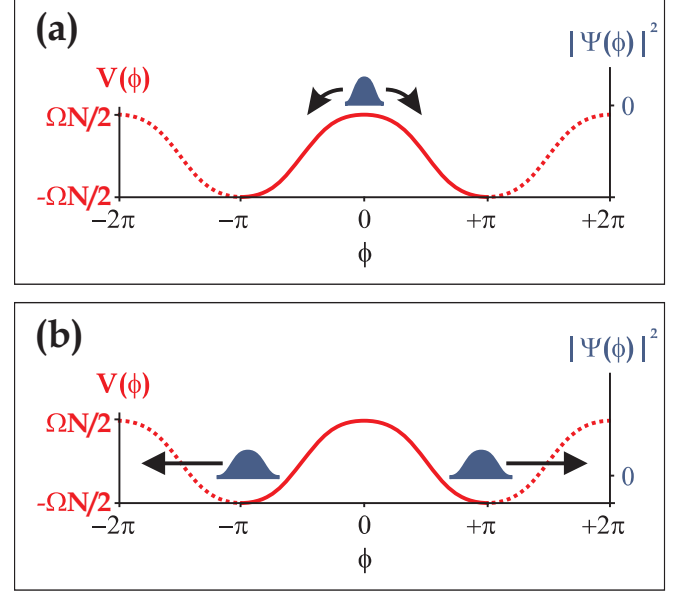


FIG. 1: Schematic time evolution using the phase-model. (a) The initial state is a Gaussian wave packet centered at a maximum of the phase potential. (b) The time evolution according to H_ϕ splits the wave packet into a superposition of two wave packets moving in opposite direction.

A. Hamiltonian

We consider a two component BEC consisting of N atoms in two different hyperfine states $|A\rangle$ and $|B\rangle$ coupled by a Raman laser or microwave field (internal Josephson effect [22, 23, 24]). The Hamiltonian of this system is given by

$$H = H_A + H_B + H_{\text{ext}}, \quad (4)$$

where H_A and H_B describe the two component condensate and H_{ext} the interaction with the external field. In second quantization the terms are given by ($\hbar \equiv 1$)

$$H_k = \int d^3 \mathbf{r} \Psi_k^\dagger \left[-\frac{\nabla^2}{2m} + V_k + \sum_l \frac{U_{kl}}{2} \Psi_k^\dagger \Psi_k \right] \Psi_k, \quad (5)$$

$$H_{\text{ext}} = \frac{1}{2} \int d^3 \mathbf{r} \left[\Psi_A^\dagger \Psi_B \Omega_R e^{-i\Delta t} + \Psi_B^\dagger \Psi_A \Omega_R^* e^{+i\Delta t} \right].$$

Here $\Psi_k \equiv \Psi_k(\mathbf{r})$ ($k = \{A, B\}$) are bosonic field operators that annihilate a particle at position \mathbf{r} in the hyperfine state $|k\rangle$. The trapping potential for atoms in state k is denoted by $V_k \equiv V_k(\mathbf{r})$ and their mass is m . The interaction strengths are given by U_{AA}, U_{BB} and U_{AB} for collisions between particles in state A, B and interspecies collisions, respectively. The effective Rabi frequency Ω_R is assumed to be positive, real, and position independent, i.e., we neglect the momentum transfer induced by the external field. The detuning of the field from resonance is denoted by Δ .

1. Two mode approximation

We assume that the spatial degrees of freedom can be described using one spatial mode function for each component [12, 14, 26]

$$\Psi_A(\mathbf{r}) = a\psi_A(\mathbf{r}) \quad \text{and} \quad \Psi_B(\mathbf{r}) = b\psi_B(\mathbf{r}), \quad (6)$$

where $\psi_k(\mathbf{r})$ are real normalized wave functions and $a, (b)$ are bosonic annihilation operators destroying a particle in the internal state $A, (B)$. They obey the usual bosonic commutation relations $[a, a^\dagger] = 1, [b, b^\dagger] = 1, [a, b] = 0$ and $[a, b^\dagger] = 0$.

2. Angular momentum representation

We use the angular momentum operators $\mathbf{S} = (\mathbf{S}_x, \mathbf{S}_y, \mathbf{S}_z)$ defined in Eq. (2) and the eigenstates of S_z with eigenvalue n :

$$|n\rangle_z = \frac{(a^\dagger)^{N/2+n} (b^\dagger)^{N/2-n}}{\sqrt{(N/2+n)! (N/2-n)!}} |\text{vac}\rangle, \quad (7)$$

The operators \mathbf{S} fulfill the standard angular momentum commutation relations $[S_i, S_j] = iS_k$, with i, j, k cyclic. From the Heisenberg uncertainty principle we find $\langle \Delta S_i^2 \rangle \langle \Delta S_j^2 \rangle \geq \frac{1}{4} |\langle S_k \rangle|^2$.

3. Two mode Hamiltonian

Using Eqs. (2,6) the Hamiltonian reduces (up to a constant) to

$$H = \delta S_z + \chi S_z^2 + \Omega S_x, \quad (8)$$

where $\delta = \omega_A - \omega_B + \Delta + (u_{AA} - u_{BB})(N - 1)/2$, and $\chi = (u_{AA} + u_{BB} - 2u_{AB})/2$ with . The single particle ground state energies ω_A and ω_B , the coupling u_{kl} and the effective Rabi frequency Ω are given by

$$\begin{aligned} \omega_k &= \int d^3\mathbf{r} \psi_k^* \left[-\frac{\nabla^2}{2m} + V_k \right] \psi_k, \\ u_{kl} &= U_{kl} \int d^3\mathbf{r} |\psi_k|^2 |\psi_l|^2, \\ \Omega &= \Omega_R \int d^3\mathbf{r} \psi_A^* \psi_B. \end{aligned} \quad (9)$$

In the following we will consider the situation, where $\chi > 0$ and $\delta = 0$.

B. Phase model

In the introduction we used the phase model [21, 22] to qualitatively explain how the time evolution according to H can be deployed to create many particle entangled

states. To be more precise the continuous eigenstates of ϕ are given by

$$|\phi\rangle = \frac{1}{\sqrt{2\pi}} \sum_{n=-N/2}^{+N/2} e^{-in\phi} |n\rangle_z. \quad (10)$$

Using the relation $S_z |\phi\rangle = -i\partial_\phi |\phi\rangle$, neglecting terms of order $1/N$ and for $\Omega \ll N\chi/2$ we can rewrite the Hamiltonian H [21] in the phase representation as given in Eq. (3). The Hamiltonian H_ϕ describes a single fictitious particle moving as a pendulum [24, 25]. The first term of H_ϕ can easily be identified as the kinetic energy of the particle and the second term is a conservative periodic potential. For large $N \gg 1$ the initial phase wave function $\Psi(0, \phi) \equiv \langle \phi | \Psi(t=0) \rangle$ is well approximated by a narrow gaussian wave-packet

$$\begin{aligned} \Psi(0, \phi) &= \frac{1}{\sqrt{2^{N+1}\pi}} \sum_{n=-N/2}^{+N/2} \binom{N}{N/2-n}^{1/2} e^{in\phi} \\ &\approx (2\pi\sigma^2)^{-1/4} e^{-\frac{\phi^2}{4\sigma^2}}. \end{aligned} \quad (11)$$

The width of the Gaussian is $\sigma = 1/\sqrt{N}$. The phase model is valid for $\Omega \ll \chi N$ [21]. Since we do not want to restrict ourselves to this case we will now derive a semiclassical model valid for arbitrary Ω .

C. Semiclassical model

The many particle entangled state we are interested in are superposition states of two wave packets centered at two different relative particle numbers. We want to use a semiclassical model to estimate the position of the maxima of these wave packets. We assume the collective spin \mathbf{S} to behave like a classical quantity, which is possible if the discreteness of the energy levels is negligible i.e. for $N \gg 1$. Furthermore the semiclassical treatment will only be valid as long as interference effects are negligible. For the initial state we consider it will turn out that such interference effects become important for times $t > 2t_c$, where t_c defined in Eq. (30) is the time it takes to create the many particle entangled state.

Under these conditions we replace the spin operator \mathbf{S} by c-numbers

$$\mathbf{S} \rightarrow \frac{N}{2} (\sin \theta \cos \phi, \sin \theta \sin \phi, \cos \theta). \quad (12)$$

This implies the factorization of expectation values of products of operators like e.g. $\langle \{S_x, S_y\} \rangle$ by $2 \langle S_x \rangle \langle S_y \rangle$. From the Heisenberg equations of motion for the operator \mathbf{S} given by

$$\frac{d}{dt} \begin{pmatrix} S_x \\ S_y \\ S_z \end{pmatrix} = \begin{pmatrix} -\chi \{S_z, S_y\} \\ \chi \{S_z, S_x\} - \Omega S_z \\ \Omega S_y \end{pmatrix} \quad (13)$$

we obtain for the time evolution of the angles θ, ϕ

$$\frac{d}{dt} \begin{pmatrix} \theta \\ \phi \end{pmatrix} = \frac{\chi N}{2} \begin{pmatrix} -\omega \sin \phi \\ 2 \cos \theta - \omega \cot \theta \cos \phi \end{pmatrix}, \quad (14)$$

with $\omega \equiv 2\Omega/\chi N$. The corresponding vector fields are shown in Fig. 2 for different values of ω .

From the continuous Wigner function W_t [29] defined as the Fourier transform of the quantum characteristic function \tilde{W}_t given by

$$\begin{aligned} W_t(n, \phi) &= (2\pi)^{-2} \int d\phi' \int dn' \tilde{W}_t(n', \phi') e^{+i(\phi' n - n' \phi)}, \\ \tilde{W}_t(n', \phi') &= \langle \Psi(t) | e^{i(n' \hat{\phi} - \phi' S_z)} | \Psi(t) \rangle, \end{aligned} \quad (15)$$

we get the initial Liouville distribution on the sphere as

$$P_{t=0}(\theta, \phi) = \frac{1}{\sin \theta} W_{t=0}(n = S \cos \theta, \phi). \quad (16)$$

For the initial state $|\Psi(t=0)\rangle$ the Liouville distribution is well approximated by a Gaussian of narrow radial width $\sigma = 1/\sqrt{N}$:

$$P_0(\theta, \phi) = \mathcal{N} e^{-\frac{2}{\sigma^2 N^2} (\mathbf{S} - \mathbf{S}_0)^2} \approx \frac{1}{2\pi\sigma^2} e^{-\frac{1}{2\sigma^2} (\cos^2 \theta + \phi^2)}. \quad (17)$$

The semiclassical time evolution of the Liouville distribution is then given by

$$\begin{aligned} P_t(\theta, \phi) &= \frac{1}{\sin \theta} \int d\theta' \sin \theta' \int d\phi' P_0(\theta', \phi') \times \\ &\quad \delta(\theta - \tilde{\theta}_t(\theta', \phi')) \delta(\phi - \tilde{\phi}_t(\theta', \phi')), \end{aligned} \quad (18)$$

where $\tilde{\theta}_t(\theta', \phi')$, $\tilde{\phi}_t(\theta', \phi')$ are the classical trajectories of a fictional particle starting at $t = 0$ from θ', ϕ' , i.e. solutions of Eq. (14). The semiclassical expectation value of an operator $C(\mathbf{S})$ is given by

$$\begin{aligned} \langle C(\mathbf{S}) \rangle_t &= \int_0^\pi d\theta \sin \theta \int_{-\pi}^{+\pi} d\phi P_t(\theta, \phi) \\ &\quad C \left[\frac{N}{2} (\sin \theta \cos \phi, \sin \theta \sin \phi, \cos \theta) \right]. \end{aligned} \quad (19)$$

III. ENGINEERING MANY-PARTICLE ENTANGLED STATES

In this section we first define different kinds of many particle entangled states and review several schemes for engineering entanglement in two component BECs. We then study in detail a scheme which allows the production of a many particle entangled state in a two component BEC at a time scale proportional to $1/N$.

A. Many particle states

We introduce different kinds of many particle states which will be used to characterize the states encountered in the numerical calculations performed in the subsequent section V.

1. Coherent spin states (CSS)

The CSS [28] are eigenstates of the angular momentum operator $S_{\mathbf{n}_1} \equiv \mathbf{n}_1 \cdot \mathbf{S}$ with eigenvalue $N/2$, where \mathbf{n}_1 is a unit vector pointing in the direction (θ, ϕ) . These states are completely uncorrelated and can be written as a separable product of single-particle states given by

$$\begin{aligned} |\theta, \phi\rangle &\equiv e^{-iS_z\phi} e^{-iS_y\theta} |+N/2\rangle_z \\ &= \frac{1}{\sqrt{N!}} \left[\cos \frac{\theta}{2} e^{-i\phi/2} a^\dagger + \sin \frac{\theta}{2} e^{+i\phi/2} b^\dagger \right]^N |vac\rangle \\ &= \left[\cos \frac{\theta}{2} e^{-i\phi/2} |A\rangle + \sin \frac{\theta}{2} e^{+i\phi/2} |B\rangle \right]^{\otimes N}. \end{aligned} \quad (20)$$

CSS are minimum uncertainty states with $\langle \Delta S_{\mathbf{n}_3}^2 \rangle = \langle \Delta S_{\mathbf{n}_3}^2 \rangle = N/4$, where $\mathbf{n}_1, \mathbf{n}_2, \mathbf{n}_3$ are unit vectors orthogonal to each other.

2. Spin squeezed states (SSS)

The SSS [30, 31] are characterized by a reduced variance compared to that of the CSS in one of the spin-components $S_{\mathbf{n}_2}$ or $S_{\mathbf{n}_3}$ whereas the variance in the other orthogonal component is correspondingly enhanced. The amount of squeezing is determined by the squeezing parameter ξ given by

$$\xi^2 = \min_{\mathbf{n}_{1,2,3}} \frac{N(\Delta S_{\mathbf{n}_1})^2}{\langle S_{\mathbf{n}_2} \rangle^2 + \langle S_{\mathbf{n}_3} \rangle^2}, \quad (21)$$

If $\xi^2 < 1$ the state of the atoms is non-separable (i.e. entangled) as has been shown in [12]. The parameter ξ^2 thus characterizes the atomic entanglement, and we refer to states with $\xi^2 < 1$ as “spin squeezed states”.

We also note that this parameter determines the amount of noise-reduction in atomic clocks [31]. Therefore the robust creation [12] and preservation [22] of SSS might prove useful in enhancing the accuracy of these atomic clocks.

3. Maximally entangled states (MES)

A second type of macroscopically entangled states can be written as

$$|\text{GHZ}\rangle_N = \frac{1}{\sqrt{2}} (|A\rangle^{\otimes N} + |B\rangle^{\otimes N})$$

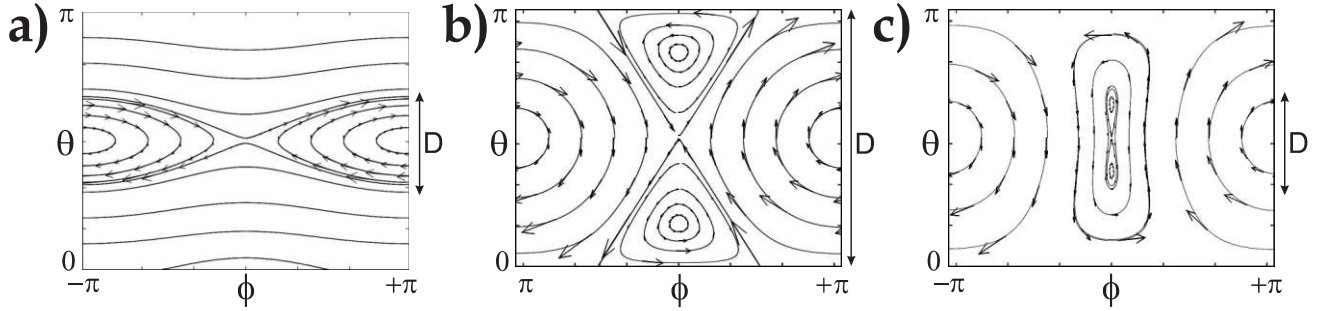


FIG. 2: Vector field (arrows) and trajectories (solid curves) of Eq. (14) for three different coupling strengths: a) $\omega = 0.14$, b) $\omega = 1$ and c) $\omega = 1.87$, where $\omega \equiv 2\Omega/\chi N$.

$$\begin{aligned}
 &= \frac{1}{\sqrt{2}} (|+N/2\rangle_z + |-N/2\rangle_z) \\
 &= \frac{1}{\sqrt{2}} (|\theta = 0, \phi = 0\rangle + |\theta = \pi, \phi = 0\rangle) \quad (22)
 \end{aligned}$$

They are a generalization for N particles of the well known GHZ-state of three particles [3, 5, 7]. As can be seen from Eq. (22) these states can be written as either a coherent superposition of N particles being in the state A and N being in state B or as a coherent superposition of two CSS pointing in opposite directions on the Bloch-sphere.

B. Schemes for producing many particle entanglement

There have been several proposals of how to engineer many particle entanglement in BECs. Basically these schemes can be divided into two different kinds. The first possibility is to engineer the ground state of the system to be an entangled state. This can be done by appropriately manipulating the interaction between the particles [26, 32]. The entangled state is then created by cooling the system to its ground state. The second possibility is to control the dynamics of the system such that an initially separable state evolves coherently into an entangled state [14, 18, 20, 33].

1. Thermodynamical Schemes

For $\chi > 0$ and $\Omega = 0$ the ground state of the Hamiltonian (1) is the number-squeezed (“dual fock”) [34] state $|0\rangle_z$, with half of the atoms in $|A\rangle$ and the others in $|B\rangle$. As first noted by Cirac *et al.* [26] for $\chi < 0$ and $|\Omega| < N/2$ the ground state of the system corresponds to an entangled state and a maximally entangled state of the form Eq. (22) is attained for zero coupling (i.e. $\Omega \rightarrow 0$). The major obstacle in cooling to the ground state is the small energy gap between the ground and the first excited state which scales like χ .

2. Dynamical Schemes

One of the simplest ways [20] to obtain a SSS is to start from a one component BEC in A (corresponding to a CSS $|N/2\rangle_{-z}$), to apply a fast $\pi/2$ pulse ($\Omega \gg \chi N$) that rotates the CSS on the Bloch sphere by an angle $\pi/2$ around the y -axis aligning it along the \mathbf{x} direction (corresponding to $|N/2\rangle_x$). The subsequent evolution due to the Hamiltonian H (with $\Omega = 0$) establishes correlations among the particles, creating an SSS with a squeezing parameter $\xi \approx (3/N)^{2/3}/2$ for large N [30] on a time scale $t \approx 2 \times 3^{1/6}/\chi N^{2/3}$. Taking into account the spatial degrees of freedom and inelastic collisions with background particles still allows for considerable squeezing of the SSS as was more recently shown in [12, 17, 27]. As noted by Mølmer *et al.* [33] and Castin [35] one-axis squeezing also provides a perfect GHZ-state at a much later time $t = \pi/2\chi$ neglecting, however, the spatial degrees of freedom and decoherence processes.

Even smaller squeezing parameters ξ can be obtained by engineering two particle interactions resulting in a Hamiltonian of the form $H_{\text{int}} = \chi(S_z^2 - S_y^2)$ as recently proposed in [14, 18] and thus implementing two-axis-squeezing [30]. In [18] intermediate molecular states of two-atoms are used to create a Hamiltonian of the form H_{int} while in [14] this is achieved by applying a series of laser pulses to the two-component BEC. As discussed by Law *et al.* [36] turning on a small coupling $\Omega \ll \chi N$ can be used to further improve the squeezing properties. Gordon *et al.* [20] showed numerically that for $\Omega \sim \chi N$ Schrödinger Cat states can be obtained on short time scales.

The main task of the remainder of this paper is to investigate in detail dynamical schemes which create many particle entangled states of the form

$$|\text{Cat}(D)\rangle_N = \frac{1}{\sqrt{2}} \left(\left| +\frac{D}{2} \right\rangle_z + \left| -\frac{D}{2} \right\rangle_z \right), \quad (23)$$

$$|\text{Cat}(\gamma)\rangle_N = \frac{1}{\sqrt{2}} \left(\left| \frac{\pi + \gamma}{2}, 0 \right\rangle + \left| \frac{\pi - \gamma}{2}, 0 \right\rangle \right), \quad (24)$$

on a time scale proportional to $1/N$ using the Hamil-

tonian H_{BEC} (see also [20]). Eq. (23) is a macroscopic superposition of eigenstates of the operator S_z characterized by a “distance” D . The other entangled state Eq. (24) is a superposition of two CSS separated by an angle γ . Note that for $D = 0$ and $\gamma = 0$ these states are not entangled, whereas for $D = N$ and $\gamma = \pi$ they coincide forming an MES.

IV. SEMICLASSICAL RESULTS

In this section we first identify three different coupling regimes, for which the evolution of the initial state has a qualitatively different behavior. Then we derive analytical approximations for the time scales on which the many particle entangled states Eq. (23) are formed, and the attainable separation D as a function of Ω . We find that for $\Omega = \chi N/2$ states close to MES are created on a time scale $t_c = \ln(8N)/\chi N$.

A. Coupling regimes

As can be seen from Fig. 2 the vector field (14) on the Bloch-sphere is qualitatively different for $2\Omega/\chi N \equiv \omega < 1$ (weak coupling regime) and $\omega > 1$ (strong coupling regime). We will thus investigate these two regimes separately and also look at the intermediate case $\omega = 1$ (critical coupling).

In the weak coupling regime the trajectories passing through the maximum of our initial distribution at $\theta = \pi/2, \phi = 0$, make a full revolution in ϕ . The separatrix separates the rotational modes of the pendulum from the oscillatory ones. The rotational modes of the pendulum rotate continuously either clockwise- or counter-clockwise (trajectories in the lower/upper half plane of θ outside the separatrix), whereas the oscillatory modes oscillate around $\phi = -\pi/2$ (trajectories inside the separatrix), as shown in Fig. 2a. In this regime the time evolution first squeezes our initial state along the separatrix. Then two elongated peaks aligned along the ϕ -axis centered at $\phi = \pm\pi$ appear, respectively (see Fig. 3a2-b2). From the reduced density distribution

$$P_{\text{sc}}(n, t) = \int d\phi \tilde{P}_t(n, \phi), \quad (25)$$

$$\tilde{P}_t(n = \cos \theta, \phi) = \sin \theta P_t(\cos \theta, \phi), \quad (26)$$

we find good agreement with the Wigner distribution for a state of the form Eq. (23) as shown in Fig. 3a4-b4.

In the strong coupling regime the trajectories passing through $\theta = \pi/2, \phi = 0$, do neither perform a full revolution in ϕ nor separate the rotational from the oscillatory modes any more as can be seen from Fig. 2c. In fact, there are no rotational modes for $\Omega > \chi S$. However, first the initial state again is squeezed like in the weak coupling regime (see Fig. 4a1,b1). Then two well separated gaussian peaks - one on the northern and another at

the southern hemisphere appear. In contrast to the weak coupling regime they are now centered at $\phi = 0$ as shown in Fig. 4a2,b2. This distribution corresponds roughly to a state of the form Eq. (24) as shown in Fig. 4b4.

B. Distance

According to the semiclassical time evolution the largest distance D of the many particle entangled state is equivalent to the largest separation of the separatrix at $\phi = \pi$ in the weak coupling regime and at $\phi = 0$ in the strong coupling regime. By using the conservation of energy $E(\theta, \phi) = \chi(N \cos(\theta)/2)^2 + \Omega N \sin(\theta) \cos(\phi)/2 = \Omega N/2$, we find the shape of the separatrix

$$\begin{aligned} \cos \phi[\theta] &= \frac{1 - \omega^{-1} \cos^2 \theta}{\sin \theta} \quad \Leftrightarrow \\ \sin \theta[\phi] &= \frac{\omega}{2} \cos \phi \pm \sqrt{\left(\frac{\omega}{2} \cos \phi\right)^2 - \omega + 1}. \end{aligned} \quad (27)$$

It follows that in the weak coupling regime the distance D is given by (cf. Appendix B)

$$D = N \sqrt{\omega(2 - \omega)}, \quad (28)$$

and in the strong coupling regime the angle between the two CSS states γ is

$$\gamma = 2 \arcsin(\sqrt{\omega(2 - \omega)}). \quad (29)$$

In the weak coupling regime the maximum distance D increases with ω until $\omega = 1$ where D takes its largest possible value $D = N$ (see Fig. 5a). Thus for $\omega = 1$ we obtain a state close to a MES. For larger couplings ($\omega > 1$) a superposition state of the form Eq. (24) is created. The angle γ decreases with increasing ω until at $\omega = 2$ no superposition is obtained according to Eq. (29). Exact numerical calculations show that for $\omega \geq 2$ macroscopically entangled states of the latter form are still obtained but with $\gamma \ll \pi$.

C. Time Scales

We will now focus on the required time t_c to create a many particle entangled state by using the semiclassical time evolution of the wave packets forming the superposition states. It is crucial that t_c is short compared to decoherence times to successfully create many particle entanglement.

The time t_c is approximately equal to the time needed to “travel” along the separatrix from the point lying at the distance σ from $\phi = 0, \theta = \pi/2$ to $\cos \theta = D/N$, i.e., the point where the many particle entangled state forms. Combining Eqs. (14,27, 28) one obtains (cf. Appendix

B)

$$\chi t_c = \frac{2 \log \left[\sqrt{2N(2-\omega)} + \sqrt{2N(2-\omega)-1} \right]}{N \sqrt{\omega(2-\omega)}} \quad (30)$$

$$\approx \frac{\log [8N(2-\omega)]}{N \sqrt{\omega(2-\omega)}},$$

where the last approximation is valid for $2N(2-\omega) \gg 1$. We notice that t_c scales as $1/N$ and reaches its minimum value for $\omega \approx 1$, i.e., near the critical coupling, see Fig. 5b.

V. NUMERICAL RESULTS

We calculated numerically the solution of the Schrödinger equation for the exact model Eq. (8) with a moderate number of particles N up to 10^3 . A comparison of the exact results with the approximations of Sec. IV yields good agreement already for $N \geq 50$. Also, we calculate the overlap of the cat-states $|\psi\rangle$ with the states defined in Eqs. (23,24), i.e., their fidelity

$$F_D = |N \langle \text{Cat}(D) | \psi \rangle|^2. \quad (31)$$

Furthermore we find a partial revival of the initial wave function at time $t \sim 2t_c$. We characterize this revival by the overlap with the initial CSS state R given by

$$R = |\langle \Psi(0) | \Psi(t) \rangle|^2 = |_x \langle N/2 | \Psi(t) \rangle|^2. \quad (32)$$

Since R turns out to be larger than $1/2$ for $0.1 < \omega < 1.9$ it is useful for measurement purposes, especially for checking the coherence of an MES, as described in detail in Sec.(VII B).

A. Comparison of Semiclassical with Exact Results

We calculate numerically the solution of the Liouville equation Eq. (18) and compare it with the exact discrete Wigner function as defined by Leonhardt [29] for $0 < \omega < 2$. From Figs. 3a1-b2, 4a1-b2 we see excellent agreement between the two results for $N \geq 50$ and $t < 2t_c$. Afterwards interference effects become important and the semiclassical model breaks down as shown in Figs. 3a3-b3, 4a3-b3. As can be seen by comparing Figs. 3a4-b4 and Figs. 3a4-b4 we obtain a revival of the initial state of about 55% [90%] for the exact solution in the weak [strong] coupling regime, whereas the overlap of the semiclassical solution with the initial state is only about 10%.

Next we proceed to check the validity of Eqs. (28,30) for D and t_c . Numerically we find D and t_c by looking for the maximum $F_D(t) > F_0(t)$. The numerical values for D and t_c agree very well with the analytical expressions Eqs. (28,30) for $N \geq 50$, see Fig. 5a,b.

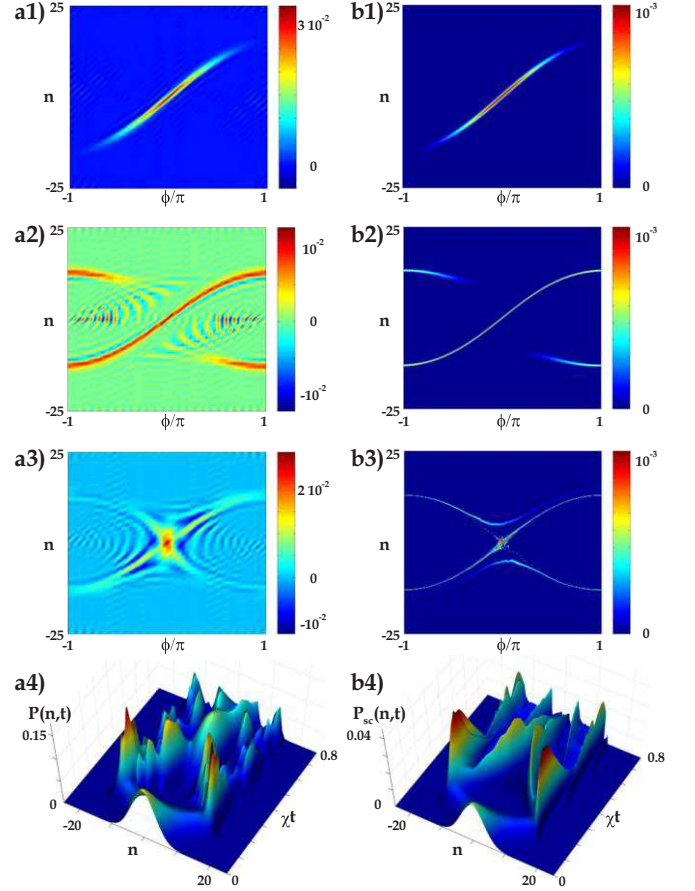


FIG. 3: Comparison of the evolution of the system for $\omega = 0.14$ (weak coupling) and $N = 50$. The exact discrete Wigner function $W_t(n, \phi)$ is plotted in (a1-a3) compared with the Liouville distribution $\tilde{P}_t(n = \cos \theta, \phi)$ in (b1-b3) at three characteristic times. 1) $t = t_c/2$ showing a SSS; 2) $t = t_c$ showing the macroscopic superpositon state; and in 3) $t \sim 2t_c$ showing the revival. a4) exact discrete number distribution $P(n, t) \equiv |z \langle n | \Psi(t) \rangle|^2$; b4) reduced density distribution $P_{sc}(n, t)$.

B. Critical Coupling

We see from Fig. 5 that for the critical coupling $\omega = 1$ we obtain the largest possible $D = N$, a short creation time t_c , the best fidelity F_D , and the largest value for the partial revival R . Also the decrease of F_D with increasing number of particles N is slowest at the critical coupling. In Fig. 7 we plot the time evolution showing the initial squeezing followed by the creation of a state close to MES and the partial revival of the initial state with $R = 79\%$.

VI. PRE-SQUEEZING

We investigate if better results for F_D are obtainable by adjusting the initial variances $\Delta S_y, \Delta S_z$ by squeez-

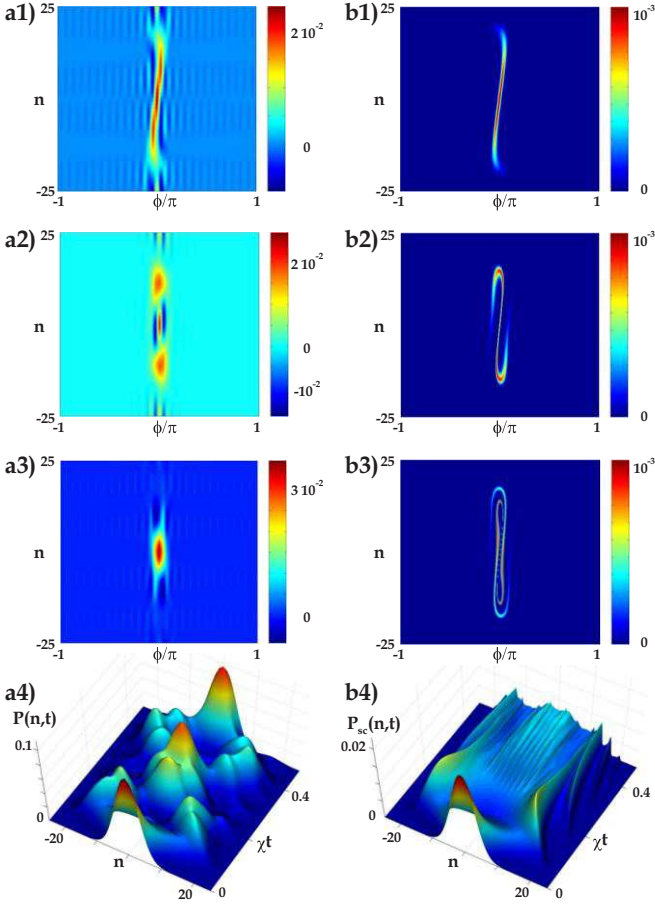


FIG. 4: Same as Fig. 3 but for $\omega = 1.87$ (strong coupling).

ing. We choose one-axis-squeezing, which is easily implemented by turning off the external field after the initial $\pi/2$ -pulse for a time τ . Afterwards a second pulse with angle α is applied before the system is evolved according to Eq. (8). We optimize τ and α for obtaining the largest F_D and restrict ourselves to the most interesting case $\omega = 1$. The results are shown in Fig. 8. A substantial improvement in the obtainable fidelity F_D can thus be reached by pre-squeezing, (cf. Fig. 8c) which, furthermore, decreases much slower with increasing N than without pre-squeezing.

VII. DISCUSSION

A. Stability under Decoherence

A major problem of creating a macroscopic entangled state is decoherence, affecting every realistic system. For instance the entanglement in an MES is destroyed by losing a single particle, as is easily shown by calculating

$$\left| \tilde{\Psi}_A \right\rangle_{\tilde{N}} = \frac{a|GHZ\rangle_N}{\|a|GHZ\rangle_N\|} = |A\rangle^{\otimes \tilde{N}} = \left| \tilde{N} : \tilde{N}/2 \right\rangle_z, \quad (33)$$

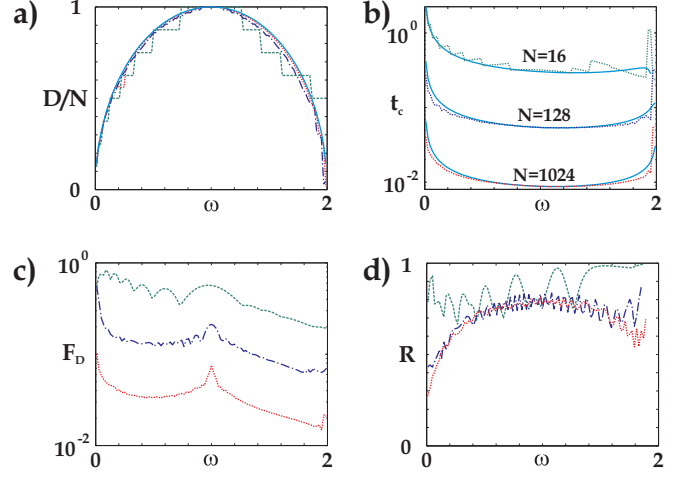


FIG. 5: Comparison of the exact with the semiclassical results. a) Attainable distance D as a function of ω , exact solution for $N = 16$ (dashed curve), $N = 128$ (dash-dotted curve), $N = 1024$ (dotted curve), and semiclassical result (solid curve). b) Time t_c as a function of ω : exact solution (dashed curves) compared with the semiclassical result (solid curves) for $N = 16, 128, 1024$. c) The maximum fidelity F_D as a function of ω . d) Revival R for $N = 16$ (dashed curve), $N = 128$ (dash-dotted curve), and $N = 512$ (dotted curve).

$$\left| \tilde{\Psi}_B \right\rangle_{\tilde{N}} = \frac{b|GHZ\rangle_N}{\|b|GHZ\rangle_N\|} = |B\rangle^{\otimes \tilde{N}} = \left| \tilde{N} : -\tilde{N}/2 \right\rangle_z \quad (34)$$

with $\tilde{N} = N - 1$ and $|N : n\rangle_z$ the eigenstate of S_z for N particles.

In our scheme, however, we expect the effects of decoherence to be reduced for two reasons. (i) The many particle entangled state is created on a very short time scale, for which we expect only few particles to be lost. (ii) Losing a single particle does not completely destroy the entanglement for $D < N$, since

$$\begin{aligned} \left| \tilde{\Psi}_A \right\rangle_{\tilde{N}} = & \frac{a|Cat(D)\rangle_N}{\|a|Cat(D)\rangle_N\|} = \frac{1}{\sqrt{2}} \left[\sqrt{1 + \frac{D}{N}} \left| \tilde{N} : \frac{D-1}{2} \right\rangle_z \right. \\ & \left. + \sqrt{1 - \frac{D}{N}} \left| \tilde{N} : -\frac{D+1}{2} \right\rangle_z \right], \end{aligned} \quad (35)$$

$$\begin{aligned} \left| \tilde{\Psi}_B \right\rangle_{\tilde{N}} = & \frac{b|Cat(D)\rangle_N}{\|b|Cat(D)\rangle_N\|} = \frac{1}{\sqrt{2}} \left[\sqrt{1 - \frac{D}{N}} \left| \tilde{N} : \frac{D+1}{2} \right\rangle_z \right. \\ & \left. + \sqrt{1 + \frac{D}{N}} \left| \tilde{N} : -\frac{D-1}{2} \right\rangle_z \right]. \end{aligned} \quad (36)$$

Recently Savage *et al.* [37] discussed the effects of decoherence due to the presence of non-condensed atoms. For low temperatures the primary effect is to introduce phase-damping, which was taken into account by a four mode model in [37]. They showed that decoherence effects are negligible for $N \approx 200$, which indicates that the present scheme could be a robust implementation for creating MES.

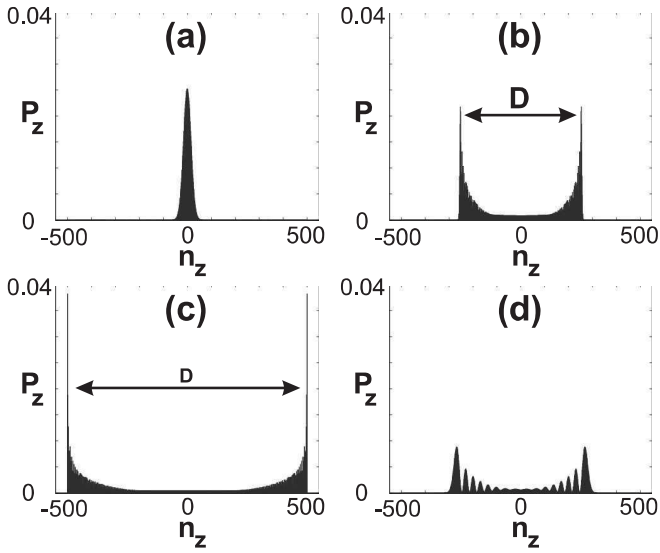


FIG. 6: Exact probability distribution $P(n, t)$ for $N = 10^3$ particles for (a) the initial state, (b) the state created for $\omega \approx 0.14$ corresponding to a distance of $D = N/2$, (c) the GHZ-like state obtained for $\omega = 1$, and (d) the state for $\omega \approx 1.87$ corresponding to an angle of $\gamma = 2 \arcsin(1/2)$.

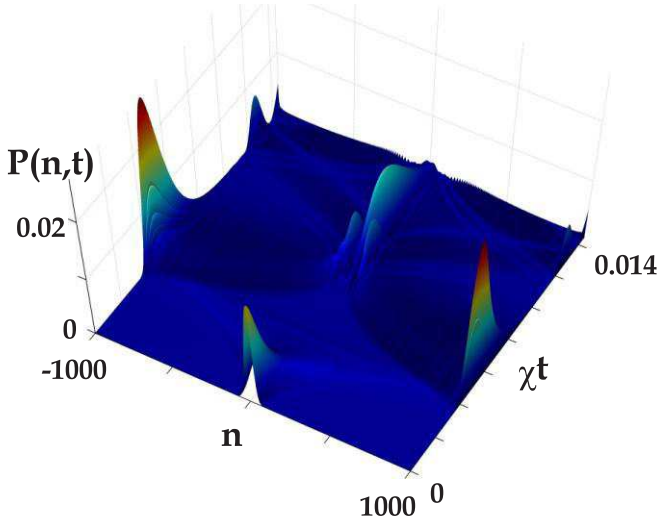


FIG. 7: Exact number distribution $P(n, t)$ as a function of n and t for $\omega = 1$ and $N = 2000$.

B. Measurement

By measuring S_z one obtains $P(n, t)$ as shown in Fig. 6. This, however, does not guarantee the state to be macroscopically entangled, since a completely incoherent mixture

$$\rho = \frac{1}{2} |D/2\rangle_z \langle D/2| + \frac{1}{2} |-D/2\rangle_z \langle -D/2| \quad (37)$$

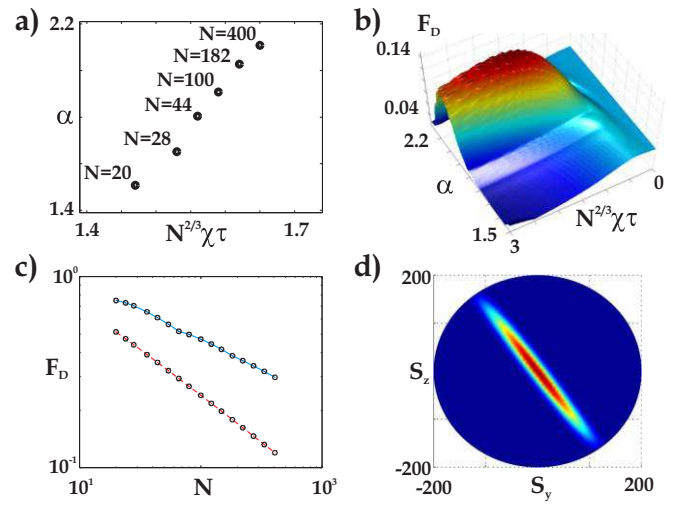


FIG. 8: a) Optimum values for τ , α for different values of N . b) Fidelity F_D as a function of τ and α for $N = 400$. c) Comparison of F_D without pre-squeezing (dash-dotted curve), and with pre-squeezing (solid curve) as a function of N , where the dots mark the numerically calculated values. d) Initial CSS-Q-function $Q(\theta, \phi) \equiv |\langle \theta, \phi | \Psi \rangle|^2$ for optimal pre-squeezing for $N = 400$.

gives the same result for $P(n, t)$. To distinguish between the two cases one has either to do density matrix tomography (endoscopy) [38, 39] or measure the purity of the system.

The latter can be realized by time reversal which can experimentally be implemented by using the external field to apply a series of pulses as shown in Appendix A. Replacing H by $-H$ after time t_c and measuring S_x after $2t_c$ the two cases can be distinguished. For the pure case one obtains always the same outcome $+N/2$, while for a mixture multiple outcomes are possible. Also the partial revival with $R > 1/2$ could be used to distinguish between the two cases without the difficulty of implementing $-H$.

C. Imperfections in the external field

Experimentally it is possible to adjust the phase β of the $\pi/2$ pulses very precisely, while it is much more difficult to exactly fulfill the condition of having a pulse area equal to $\pi/2$. Therefore we investigate the influence of errors in the pulse-area of the initial $\pi/2$ -pulse only.

The radius of the Bloch-sphere is $N/2$, while the width of the initial distribution is $\sqrt{N}/2$. Thus we expect that the required precision in the pulse area scales like $1/\sqrt{N}$. We confirmed this expectation by numerical simulation for small N up to $N \approx 10^3$.

VIII. CONCLUSION

In summary, we have investigated schemes which allow the creation of macroscopically entangled states with a distance $0 < D < N$ on time scales proportional to $1/N$. Within a semiclassical approximation we obtained analytical estimates for D and the time t_c , which are in excellent agreement with the numerical results. We also showed that the fidelity of these states can be improved significantly by one axis pre-squeezing. We estimated the effect of imperfections and decoherence, and believe that the presented scheme might be used to produce macroscopically entangled states with present state of the art technology.

Acknowledgments

This work was supported by the Austrian Science Foundation and the European Union projects under the contracts No. HPRN-CT-2000-00121 and No. HPRN-CT-2000-00125.

APPENDIX A: IMPLEMENTING THE HAMILTONIAN $-H$

First we investigate the time-evolution of H given in Eq. (8) for $\Omega \gg \chi N$. Then we show how a continuous sequence of pulses of the external field can be used to generate $-H$ which is needed to implement the measurement process discussed in Sec. VII B. For simplicity we consider the case $-H(\Omega = 0) = -\chi S_z^2$.

For $|\Omega| \gg |\chi|N$, one can neglect χS_z^2 in (8). A pulse of angle γ and phase β is characterized by

$$\int_{-\infty}^{+\infty} |\Omega(t)| dt = \gamma > 0 \quad \Omega(t) = |\Omega(t)| e^{i\beta}$$

and implements the following time-evolution

$$U_\beta(\gamma) = e^{-i\gamma[\cos(\beta)S_x - \sin(\beta)S_y]}. \quad (\text{A1})$$

Its effect corresponds geometrically to a counterclockwise rotation around the unit-vector $\mathbf{n} = (\cos(\beta), -\sin(\beta), 0)$ about an angle γ . The inverse is found by $U_\beta(\gamma)^\dagger = U_\beta(-\gamma) = U_{\beta+\pi}(\gamma)$. Since a rotation about γ around the z-axis corresponds to three pulses

$$\begin{aligned} R_z(\gamma) &= e^{-i\gamma S_z} = U_0\left(\frac{\pi}{2}\right) U_{-\frac{\pi}{2}}(\gamma) U_\pi\left(\frac{\pi}{2}\right), \\ R_z(\gamma)^\dagger &= R_z(-\gamma) = U_0\left(\frac{\pi}{2}\right) U_{\frac{\pi}{2}}(\gamma) U_\pi\left(\frac{\pi}{2}\right), \end{aligned} \quad (\text{A2})$$

a rotation around an arbitrary vector $\mathbf{n} = (\sin \theta \cos \phi, \sin \theta \sin \phi, \cos \theta)$ about an angle γ is given by

$$R_{\mathbf{n}}(\gamma) = e^{-i\gamma \mathbf{n} \cdot \mathbf{S}} = U_{-\phi-\frac{\pi}{2}}\left(\frac{\theta}{2}\right) R_z(-\phi) U_{-\phi+\frac{\pi}{2}}\left(\frac{\theta}{2}\right). \quad (\text{A3})$$

The time evolution operator U at time $t = M\tau$ after M arbitrary rotations is given by

$$\begin{aligned} U(t) &= U_{\text{ps}}(\tau)^M = \prod_{k=1}^M U_{\text{ps}}(\tau) \quad \text{with} \\ U_{\text{ps}}(\tau) &= \prod_{j=1}^J R_{\mathbf{n}_j}(\gamma_j)^\dagger e^{-i\chi S_z^2 \tau / J} R_{\mathbf{n}_j}(\gamma_j) = e^{-iH_{\text{eff}} \tau}. \end{aligned}$$

By combining two rotations about around axes $\mathbf{n}_1, \mathbf{n}_2$ ($J = 2$) we obtain $H_{\text{eff}} = \chi(S_{\mathbf{n}_1}^2 + S_{\mathbf{n}_2}^2)/2$, since

$$\begin{aligned} U_{\text{ps}}(\tau) &= e^{-i\chi S_{\mathbf{n}_1}^2 \tau / 2} e^{-i\chi S_{\mathbf{n}_2}^2 \tau / 2} \approx (1 - i\chi S_{\mathbf{n}_1}^2 \tau / 2) \times \\ &(1 - i\chi S_{\mathbf{n}_2}^2 \tau / 2) \approx e^{-i\chi(S_{\mathbf{n}_1}^2 + S_{\mathbf{n}_2}^2) \tau / 2} \quad (\text{A4}) \end{aligned}$$

to first order in τ . Thus $H_{\text{eff}} = -H$ can be implemented (up to a constant) by choosing $\mathbf{n}_1 = (1, 0, 0), \mathbf{n}_2 = (0, 1, 0)$ and making use of the identity

$$\mathbf{S}^2 = S_x^2 + S_y^2 + S_z^2 = \frac{N}{2} \frac{N+2}{2}. \quad (\text{A5})$$

APPENDIX B: SEMICLASSICAL CALCULATIONS

In this appendix we will derive the approximations of Sec. IV. First we derive the maximal distance D given in Eq. (28) for $\sigma \rightarrow 0$, then we calculate the time t_c given in Eq. (30) needed to create the macroscopic superposition states. For simplicity we restrict θ, ϕ to the intervals $0 \leq \theta \leq \pi, -\pi \leq \phi \leq \pi$ in Eqs. (27,14). Therefore we have to distinguish for the \pm sign in the second relation of Eq. (27) for the two regimes of interest, i.e. for $\omega \leq 1$ only the $+$ sign holds, whereas for $\omega > 1$ both signs hold.

For $\sigma \rightarrow 0$ D corresponds to the maximum separation along the separatrix for given ϕ , i.e.

$$D = \max_{\phi[\theta]} N \cos \theta. \quad (\text{B1})$$

Using Eq. (27) we obtain the maximum value for $\omega \leq 1$ at $\phi = \pi$ as

$$\begin{aligned} D &= N \cos \theta^+[\phi = \pi] = N \sqrt{1 - (\sin \theta^+[\phi = \pi])^2} \\ &= N \sqrt{1 - \left(\frac{-\omega + |\omega - 2|}{2}\right)^2} = N \sqrt{\omega(2 - \omega)}. \end{aligned}$$

Similarly for $1 \leq \omega \leq 2$ we obtain three values for θ at $\phi = 0$ given by $\theta_0 = 0$ and the points of maximum separation θ_\pm for the minus sign in Eq. (27). The separation γ is given by

$$\begin{aligned} \gamma &= \theta_+^- - \theta_-^- = \pi - 2 \arcsin\left(-\frac{\omega}{2} - \frac{|\omega - 2|}{2}\right) \\ &= \pi - 2 \arcsin(\omega - 1) = 2 \arcsin\left(\sqrt{\omega(2 - \omega)}\right) \quad (\text{B2}) \end{aligned}$$

Next we calculate the time t_c given in Eq. (30). Using Eq. (14) and the conservation of energy as stated in Sec. IV B we obtain $d\theta/dt$ along the separatrix for $0 \leq \theta \leq \pi/2, 0 \leq \phi \leq \pi$, as

$$\frac{d\theta}{dt} = -\chi \frac{N}{2} \sin \phi = -\chi \frac{N}{2} \sqrt{1 - \left(\frac{\omega - \cos^2 \theta}{\omega \sin \theta} \right)^2}. \quad (\text{B3})$$

Integrating this ordinary differential equation gives

$$\begin{aligned} \chi t &= -\frac{2}{N\omega} \int_{\theta(0)}^{\theta(t)} d\theta' \left[1 - \left(\frac{1 - \omega^{-1} \cos^2 \theta}{\sin \theta} \right)^2 \right]^{-1/2} \\ &= \frac{2}{N\omega} \int_{z(0)}^{z(t)} dz \left[1 - z^2 - (1 - \omega^{-1} z^2)^2 \right]^{-1/2} \\ &= \frac{2}{N\sqrt{\omega(2-\omega)}} \log \left[\frac{z(t)}{z(0)} \frac{1 + \sqrt{1 - z(0)^2/\omega(2-\omega)}}{1 + \sqrt{1 - z(t)^2/\omega(2-\omega)}} \right] \end{aligned} \quad (\text{B4})$$

where $z(t) \equiv \cos \theta(t)$. For a point on the separatrix at

a distance σ from $\theta = \pi/2, \phi = 0$, i.e. the peak of the initial distribution, $z(0)$ is obtained from the relation

$$\begin{aligned} \sigma^2 &= 4(\mathbf{S} - \mathbf{S}(0))^2 / N^2 = 2(1 - \sin \theta \cos \phi) \\ &= 2 \cos^2 \theta / \omega = 2z(0)^2 / \omega. \end{aligned} \quad (\text{B5})$$

The time needed to travel from $z(0) = \sqrt{\omega/2\sigma}$ to $z(t) = D/N = \sqrt{\omega(2-\omega)}$, i.e. the point of maximum separation of the two number state [gaussian distributions] forming the macroscopic superposition state (23,24) is then obtained using Eq. (B4) as

$$\begin{aligned} \chi t &= \frac{2}{N\sqrt{\omega(2-\omega)}} \log \frac{1 + \sqrt{1 - \sigma^2/2(2-\omega)}}{\sqrt{\sigma^2/2(2-\omega)}} \\ &= \frac{2 \log \left[\sqrt{2(2-\omega)/\sigma^2} + \sqrt{2(2-\omega)/\sigma^2 - 1} \right]}{N\sqrt{\omega(2-\omega)}} \end{aligned} \quad (\text{B6})$$

Finally using $\sigma = 1/\sqrt{N}$ we obtain Eq. (30).

[1] C. A. Sackett, D. Kielpinski, B. E. King, C. Langer, V. Meyer, C. J. Myatt, M. Rowe, Q. A. Turchette, W. M. Itano, D. J. Wineland, C. Monroe, *Nature* **404**, 256 (2000).
[2] A. Rauschenbeutel, G. Nogues, S. Osnaghi, P. Bertet, M. Brune, J. Raimond, and S. Haroche, *Science* **288**, 2024 (2000).
[3] D. Bouwmeester, J. -W. Pan, M. Daniell, H. Weinfurter, and A. Zeilinger, *Phys. Rev. Lett.* **82**, 1345 (1999).
[4] B. Julsgaard, A. Kozhekin, E. S. Polzik, *Nature* **413**, 400 (2001).
[5] C. H. Bennett, S. Popescu, D. Rohrlich, J. A. Smolin, and A. V. Thapliyal, *Phys. Rev. A* **63**, 012307 (2001).
[6] A. Einstein, B. Podolsky, and N. Rosen, *Phys. Rev.* **47**, 777 (1935).
[7] D. M. Greenberger, M. A. Horne, and A. Zeilinger, *Phys. Today* **46** (8), 22 (1993); D. M. Greenberger, M. A. Horne, and A. Zeilinger, in *Bell's Theorem, Quantum Theory and Conceptions of the Universe*, edited by M. Kafatos (Kluwer Academic, Dordrecht, 1989), p. 107; D. M. Greenberger, M. Horne, A. Shimony, and A. Zeilinger, *Am. J. Phys.* **58**, 1131 (1990).
[8] J. S. Bell, *Speakable and Unspeakable in Quantum Mechanics* Cambridge University Press, New York, 1987).
[9] E. Schrödinger, *Naturwissenschaften* **23**, 807 (1935); 823 (1935); 844 (1935).
[10] A. Zeilinger, *Phys. World* **11** (3), 35 (1998); W. Tittel, G. Ribordy, and N. Gisin, *Phys. World* **11** (3), 41 (1998); D. Deutsch and A. Ekert, *Phys. World* **11** (3), 47 (1998); D. DiVincenzo and B. Terhal, *Phys. World* **11** (3), 53 (1998).
[11] J.R. Anglin and W. Ketterle, *Nature*, **416**, 211 (2002).
[12] A. Sørensen, L. -M. Duan, J. I. Cirac, and P. Zoller, *Nature* **409**, 63-66 (2001).
[13] H. Pu and P. Meystre, *Phys. Rev. Lett.* **85**, 3987 (2000).
[14] L.-M. Duan, A. Sørensen, J. I. Cirac, and P. Zoller, *Phys. Rev. Lett.* **85**, 3991 (2000).
[15] L.-M. Duan, J. I. Cirac, P. Zoller, *Phys. Rev. A* **65**, 033619 (2002).
[16] N.P. Bigelow, *Nature* **409**, 27 (2001).
[17] U. V. Poulsen, and K. Mølmer, *Phys. Rev. A* **64**, 013616 (2001).
[18] K. Helmerson and L. You, *Phys. Rev. Lett.* **87**, 170402 (2001).
[19] D. S. Hall, M. R. Matthews, C. E. Wieman, and E. A. Cornell, *Phys. Rev. Lett.* **81**, 1543 (1998);
[20] D. Gordon and C. M. Savage, *Phys. Rev. A* **59**, 4623 (1999).
[21] see, for example, C. Menotti, J. R. Anglin, J. I. Cirac, and P. Zoller, *Phys. Rev. A* **63**, 23601 (2001).
[22] D. Jaksch, S. A. Gardiner, K. Schulze, J. I. Cirac, and P. Zoller, *Phys. Rev. Lett.* **86**, 4733 (2001).
[23] W. Zwerger, *Phys. Rev. B* **35**, 4737 (1987).
[24] A. J. Leggett, *Rev. of Mod. Phys.* **73**, 307 (2001).
[25] A. Smerzi, S. Fantoni, S. Giovanazzi, and S. R. Shenoy, *Phys. Rev. Lett.* **79**, 4950 (1997); S. Raghavan, A. Smerzi, S. Fantoni, and S. R. Shenoy, *Phys. Rev. A* **59**, 620 (1999).
[26] J. I. Cirac, M. Lewenstein, K. Mølmer, and P. Zoller, *Phys. Rev. A* **57**, 1208 (1997).
[27] A. S. Sørensen, *Phys. Rev. A* **65**, 043610 (2002).
[28] A. Perelomov, *Generalized coherent states and their applications*, Springer-Verlag (1986).
[29] U. Leonhardt, *Phys. Rev. A* **53**, 2998 (1996); A. Vourdas, *Phys. Rev. A* **41**, 1653 (1990).
[30] M. Kitagawa and M. Ueda, *Phys. Rev. A* **47**, 5138 (1993).
[31] D. J. Wineland, J. J. Bollinger, W. M. Itano, and D. J. Heinzen, *Phys. Rev. A* **50**, 67 (1994).
[32] C. P. Search, A. G. Rojo, and P. R. Berman, *Phys. Rev. A* **64**, 013615 (2001).
[33] K. Mølmer, and A. Sørensen, *Phys. Rev. Lett.* **82**, 1835-38 (1999).
[34] P. Bouyer, and M. A. Kasevich, *Phys. Rev. A* **56**, R1083 (1997).

- [35] Y. Castin, in *Coherent atomic matter waves*, Lecture Notes of Les Houches Summer School, p. 1-136, edited by R. Kaiser, C. Westbrook, and F. David, EDP Sciences and Springer-Verlag (2001).
- [36] C. K. Law, H. T. Ng, and P. T. Leung, Phys. Rev. A **63**, 055601 (2001).
- [37] P. J. Y. Louis, P. M. R. Brydon, and C. M. Savage, Phys. Rev. A **64**, 053613 (2001)
- [38] R. Walser, J. I. Cirac, and P. Zoller, Phys. Rev. Lett. **77**, 2658 (1996).
- [39] P. J. Bardsley, C. Leichtle, G. Schrade, and W. P. Schleich, Phys. Rev. Lett. **77**, 2198-2201 (1996).